



## Influence of solution composition on fouling of anion exchange membranes desalinating polymer-flooding produced water

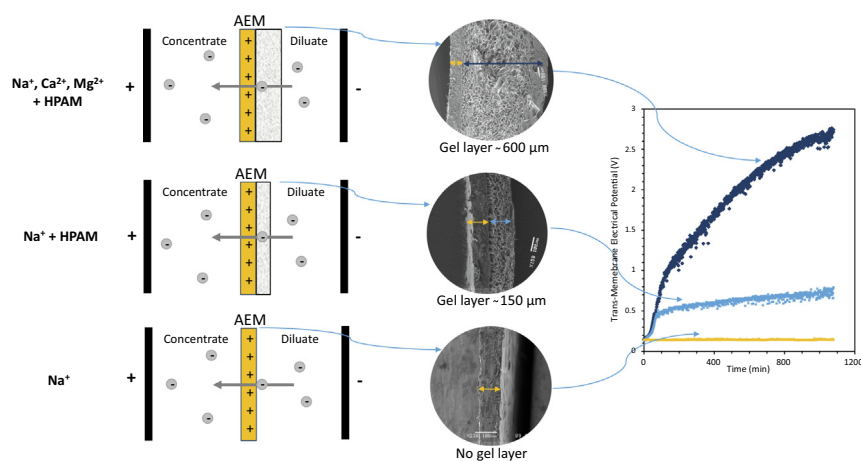
P.A. Sosa-Fernandez<sup>a,b,\*</sup>, S.J. Miedema<sup>a</sup>, H. Bruning<sup>b</sup>, F.A.M. Leermakers<sup>c</sup>, H.H.M. Rijnaarts<sup>b</sup>, J.W. Post<sup>a</sup>

<sup>a</sup>Wetsus, European Centre of Excellence for Sustainable Water Technology, P.O. Box 1113, 8911 CC Leeuwarden, Netherlands

<sup>b</sup>Environmental Technology, Wageningen University & Research, P.O. Box 8129, 6700 EV Wageningen, Netherlands

<sup>c</sup>Physical Chemistry and Soft Matter, Wageningen University & Research, P.O. Box 8038, 6700 EK Wageningen, Netherlands

### GRAPHICAL ABSTRACT



### ARTICLE INFO

#### Article history:

Received 19 July 2019

Revised 6 September 2019

Accepted 8 September 2019

Available online 12 September 2019

#### Keywords:

Membrane fouling

Electrodialysis

Polymer-flooding produced water

Partially hydrolyzed polyacrylamide

Polyelectrolyte

Concentration polarization

### ABSTRACT

**Hypothesis:** Anion exchange membranes (AEMS) are particularly prone to fouling when employed to desalinate polymer flooding produced water (PFPW), an abundant sub-product from the oil and gas industry. The formation of fouling on an AEM will be affected by the composition of the solution, which includes various dissolved salts, partially hydrolyzed polyacrylamide (HPAM), crude oil, and surfactants. **Experiments:** Electrodialysis experiments were performed to desalinate feed solutions with different compositions, aiming to distinguish between their individual and combined effects. The solutions contained diverse mono- and divalent ions. The analysis included data collected during the desalination and characterization of the fouled AEMs by diverse analytical techniques.

**Findings:** HPAM produced the most severe effects in terms of visible fouling and increase of resistance. This polyelectrolyte fouls the AEM by adsorbing on its surface and by forming a viscous gel layer that

**Abbreviations:** AEM, Anion exchange membrane; AFM, Atomic force microscopy; BW, Brackish water; CEM, Cation exchange membrane; CTAB, Cationic cetyltrimethylammonium bromide; DBL, Diffusion boundary layer; ED, Electrodialysis; EDX, Energy-dispersive X-ray spectroscopy; HPAM, Partially hydrolyzed polyacrylamide; IEM, Ion exchange membrane; PFPW, Polymer-flooding produced water; SEM, Scanning electron microscopy; TMEP, Transmembrane electric potential.

\* Corresponding author.

E-mail addresses: [paulina.sosafernandez@wetsus.nl](mailto:paulina.sosafernandez@wetsus.nl) (P.A. Sosa-Fernandez), [harry.bruning@wur.nl](mailto:harry.bruning@wur.nl) (H. Bruning), [frans.leermakers@wur.nl](mailto:frans.leermakers@wur.nl) (F.A.M. Leermakers), [huub.rijnaarts@wur.nl](mailto:huub.rijnaarts@wur.nl) (H.H.M. Rijnaarts), [jan.post@wetsus.nl](mailto:jan.post@wetsus.nl) (J.W. Post).

<https://doi.org/10.1016/j.jcis.2019.09.029>

0021-9797/© 2019 The Author(s). Published by Elsevier Inc.

This is an open access article under the CC BY-NC-ND license (<http://creativecommons.org/licenses/by-nc-nd/4.0/>).

Gel layer  
Crude oil

hampers the replenishment of ions from the bulk solution. Ca and Mg have a large influence on the formation of thick HPAM gel layers, while the oily compounds have only a minimal influence acting mainly as a destabilizing agent. The membranes also presented scaling consisting of calcium precipitates. The effects of the gel layer were minimized by applying current reversal and foulant-free solution.

© 2019 The Author(s). Published by Elsevier Inc. This is an open access article under the CC BY-NC-ND license (<http://creativecommons.org/licenses/by-nc-nd/4.0/>).

## 1. Introduction

Polymer-flooding produced water (PPFW) is an abundant stream from the oil and gas industry whose reuse can be beneficial, if adequately treated [1,2]. The stream is co-generated when polymer flooding technology is applied, which consists in injecting water viscosified with polymers into the oil reservoir, increasing the oil recovery by 5 to 30% [3]. The technology has been applied in more than 700 projects in 24 countries [4], and will likely continue to be implemented given the still increasing demand for oil [5]. This forecast also implies that large amounts of water will still be produced, provided that a single field can generate up to 75 million tons of PPFW every year [6]. Most of this water could be reused in the preparation of new polymer solutions for injection after receiving a primary treatment. However, if an additional desalination step is included after this basic treatment and the water is reused to prepare a viscous solution, the latter shows better rheological properties than solutions prepared with primary-treated PPFW or even with freshwater [1,7]. Furthermore, the desalination step is economically appealing since, in many scenarios, the savings in polymer can offset the desalination costs [8,9]. The desalination can be done via electrodialysis, a process that relies on the use of ion-exchange membranes (IEMs) and electric potential to transfer ions from a feed stream to a salty-concentrate. This technology, already operating on a pilot plant scale [1], has advantages over others because it allows the recovery of the desalted water and residual polymer in one stream [10], while the salt-containing stream still meets the requirements to be reinjected [11]. However, as for many membrane-based processes, the application of electrodialysis on a large scale is restricted by the occurrence of fouling on the IEMs [10].

Fouling is the undesirable attachment of particular substances or microorganisms to the outer or inner surface of a material [12]. The fouling occurring on IEMs when desalting PPFW causes a reduction in the desalination rates, an increase in the membrane's resistance, and a deterioration of the ion-exchange capacity [13,14]. Even after treating the PPFW with ultrafiltration [1,15], the stream still contains a variety of dissolved salts, surfactants, partially hydrolyzed polyacrylamide (HPAM), small amounts of solids in suspension and crude oil [1,11,15–17], which cause organic and inorganic fouling on the IEMs [13,14,17]. However, not all IEMs are fouled the same. The positively charged anion-exchange membranes (AEMs) are mainly fouled by the organic components, HPAM, and oil, while the negatively charged cation-exchange membranes (CEMs) are more susceptible to inorganic fouling [13]. When their individual resistance is measured, fouled AEMs presented a much higher increase compared to CEMs exposed to the same conditions [13,15]. Overall, the literature indicates that the impact of fouling by PPFW is more significant for AEMs than for CEMs, so it has been a priority of researchers to mechanistically understand and mitigate its formation.

The fouling caused by PPFW on AEMs has been studied in recent years. Guo et al. [18] carried out electrodialysis experiments of NaCl solutions with different HPAM concentrations at varying current densities, with the objective of finding the mechanism of AEM fouling by HPAM. The highest fouling phenomenon was observed

with higher HPAM concentrations at higher current densities, and SEM analyses showed that a gel layer was formed on the diluate side of the AEM. Force-distance curves measured by AFM confirmed that electrostatic forces dominated the interactions between HPAM molecules and the AEMs. Thus, they suggested that the fouling was caused by negatively charged HPAM molecules moving to the positively charged AEM under electric field, forming a gel layer near the membrane surface, and fouling the AEM due to electrostatic interaction [18]. However, a previous study by Guolin et al. [10], had determined that crude oil caused the greatest increase in membrane resistance among AEMs fouled with either suspension solution, crude oil, or HPAM. They observed the formation of a compact oil film on the surface and inside the AEM, which would affect the permeation of the membrane. Later, Wang et al. [15] opposed this, concluding that HPAM affected the desalination performance and energy consumption more significantly than the oil-related effects, and that electrostatic interaction, interface thermodynamic interaction, and molecular weight of the polymer affected the membrane fouling [15].

Nevertheless, it is also known that the fouling effect can be enhanced by the interactions between inorganic and organic components [6,14]. This was recently described in the investigation of Xia et al. [13], who found through membrane resistance measurement and SEM analyses that the HPAM and the inorganic components (salts) have a synergistic effect on the fouling of IEMs. Although the study serves as a good precedent, it only evaluated the effect of a few components at fixed concentrations, and it was mainly focused on assessing the efficiency of chemical cleaning to remove the fouling from the membranes.

Accordingly, the objective of this work was to investigate how the formation of fouling on an anion exchange membrane is affected by the different components of PPFW, and to explain why this occurs. Contrary to most of the previous works, the solutions employed in this study do not only include sodium chloride, but also other mono- and divalent ions generally present in produced water, and which are known to affect the properties of HPAM [19,20]. Different concentrations of partially hydrolyzed polyacrylamide and of oily compounds were employed. The resistance of the fouling to the application of current reversal was also evaluated.

## 2. Materials and methods

### 2.1. Materials

#### 2.1.1. Six-compartment cell and setup

Electrodialysis experiments were performed in a six-compartment cell with a four-electrode arrangement, previously described by Długolecki et al. [21]. The cell consists of six blocks containing cylindrical compartments, with the cell electrodes located at the two extremities. The compartments, numbered 1 to 6 from left to right, are separated by five ion-exchange membranes (Fig. 1). The potential difference over the middle membrane can be measured by employing two L-shaped Haber-Luggin capillaries, which are positioned on either side of the membrane pointing straight at each other. The capillaries, filled with 3 M KCl

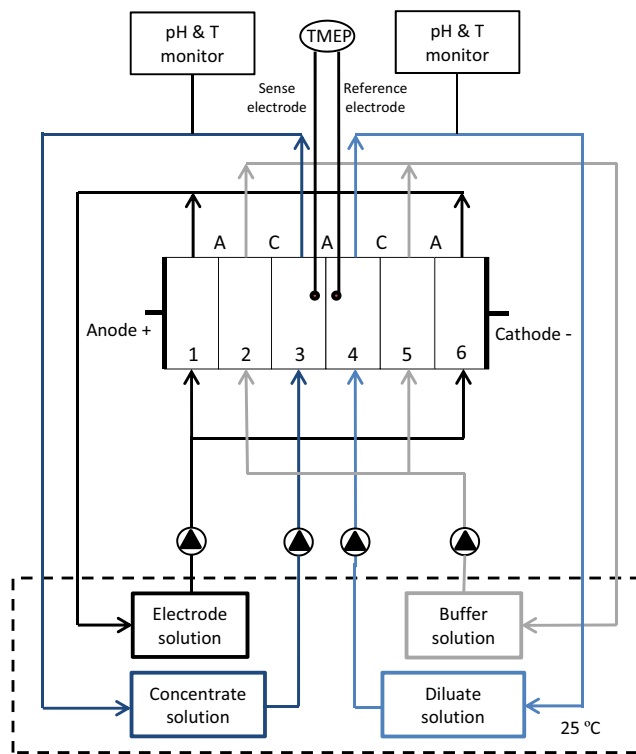


**Fig. 1.** Scheme of the six-compartment cell and setup employed to perform the electrodesialysis experiments. The transmembrane electric potential (TMEP) is measured through Haber-Luggin capillaries placed at each side of the membrane.

solution, are connected through 30 cm tubes to the glass compartments in which two reference electrodes are positioned.

The membranes were alternated as in a conventional ED cell, with the AEM under study placed in the middle. Its effective area was reduced to 7.07 cm<sup>2</sup> by placing two plastic shields on either side. The other four auxiliary membranes had an effective area of 23.8 cm<sup>2</sup>. The AEMs and CEMs employed in this study were FujiFilm type 10, kindly provided by FujiFilm Manufacturing Europe B.V. (The Netherlands), with properties summarized in Table 1.

As shown in the scheme of the setup (Fig. 1), four different solutions were employed for each experiment. 1.0 L of each solution was circulated in the following arrangement:

- Compartments 1 & 6. Electrode solution consisting of 0.05 M Na<sub>2</sub>SO<sub>4</sub>.
- Compartments 2 & 5. Buffer solution, with the same mineral composition as the feed solutions.
- Compartments 3 & 4. Concentrate and diluate solutions, respectively, with the same initial composition at each experiment.

During the experiments, the solutions were kept inside a 25 °C water bath (Julabo SW22). They were pumped through the cell at a rate of 170 mL/min by peristaltic pumps (Cole-Parmer, Masterflex L/S Digital drive, USA), and 8.0 mm PTFE tubing from EmTechnik.

**Table 1**  
Properties of the anion and cation exchange membranes employed in this study.

Membrane property	AEM type 10	CEM type 10
Backbone chemistry	Acrylamide [22]	Acrylamide
Thickness dry (μm)	125	135
Area resistance (Ω cm <sup>2</sup> )	1.7	2.0
Permselectivity (measured at 0.05–0.5 M NaCl)	95	99
pH stability	1–13	1–13

The current over the cell was applied with an Autolab PGSTAT12 (The Netherlands). This galvanostat also measured the potential over the middle (test) membrane through the two reference Ag/AgCl electrodes (QM711X, QJS, The Netherlands) and the capillaries. The pH and temperature of the diluate and concentrate solutions were monitored inline with Orbisint CPS11D-7BA21 probes connected to a Liquisys-M pH digital sensor, both from Endress + Hauser (Germany).

### 2.1.2. Preparation of solutions

Each electrodesialysis experiment made use of feed solutions with different composition, which included varied mono- and multi-valent ions, viscosifying polymer, and oily compounds [10], as shown in Table 2. The mineral composition consisted of either sodium chloride or brackish water (BW). The latter composition was based on the Marmul field, in Oman [23], and is displayed in Table 3 along with one variant. All solutions were prepared by dissolving the specified salts in demineralized water to create stock solutions, which were later employed as a basis on which to add the HPAM and/or the oily components.

The solutions with HPAM were prepared by slowly adding the dry polymer to the vortex formed on the salt solution under fast stirring. Once all the polymer was added, the stirring speed was reduced and maintained for at least 24 h to guarantee its hydration [2].

Regarding the oily compounds, two different compositions were studied: one with crude oil and one with a model emulsion. In both cases, stock solutions were prepared, characterized, and dosed to attain concentrations of 2–20 mg of oily compound per liter of test solution, as obtained after a secondary treatment [10,11].

The preparation of the model emulsion was based on the method described in [24]. In short, 346 mg of cationic cetyltrimethylammonium bromide (CTAB) surfactant were dis-

**Table 2**  
Composition of the diluate and concentrate solutions for the different fouling experiments.

Experiment	Mineral composition	HPAM polymer	Oily compounds
E1	53.3 mM NaCl	–	–
E2	53.3 mM NaCl	1.0 g/L	–
E3	77.0 mM NaCl	1.0 g/L	–
E4a, E4b*	Brackish water (BW)	1.0 g/L	–
E5	BW with 3x[Ca + Mg]	1.0 g/L	–
E6	BW only Ca (x2)	1.0 g/L	–
E7	BW only Mg (x2)	1.0 g/L	–
E8	BW	–	2 mg/L crude oil
E9	BW	0.5 g/L	2 mg/L crude oil
E10	BW	1.0 g/L	2 mg/L crude oil
E11	77.0 mM NaCl	1.0 g/L	2 mg/L crude oil
E12	BW	1.0 g/L	20 mg/L crude oil
E13	BW	1.0 g/L	20 mg/L model emulsion
E14	BW with 3x[Ca + Mg]	1.0 g/L	20 mg/L model emulsion

\* E4 was performed in duplicate.

**Table 3**  
Mineral composition of the solutions. Based on the composition reported in [23].

Components	Brackish water (BW) (mM)	BW with 3x[Ca + Mg] (mM)
NaHCO <sub>3</sub>	15.59	15.59
KCl	0.72	0.72
Na <sub>2</sub> SO <sub>4</sub>	2.51	2.51
NaCl	53.30	53.30
CaCl <sub>2</sub> *2H <sub>2</sub> O	0.65	1.96
MgCl <sub>2</sub> *6H <sub>2</sub> O	0.46	1.37

solved in 998.0 g of brackish solution previously conditioned to 45 °C. Then, 2.0 g of hexadecane was added and the solution was mixed at 14,000 rpm by an IKA T25 Ultra-Turrax emulsifying mixer (Germany) for 10 min. The emulsion had no visible phase separation, so its oil concentration was 2.0 g/L.

The stock solution with crude oil was prepared in a similar way. After heating 2.0 L of brackish solution to 45 °C, 2.0 g of crude oil was added, and the solution was mixed as described for the model emulsion. This mixture was rested for 24 h, after which the water phase was recovered and stored as oil stock solution. Its oil concentration was estimated via TOC analysis (Section 2.2.3).

All the feed solutions were prepared with analytical grade salts (NaCl, CaCl<sub>2</sub>·2H<sub>2</sub>O, MgCl<sub>2</sub>·6H<sub>2</sub>O, NaHCO<sub>3</sub>, KCl, and Na<sub>2</sub>SO<sub>4</sub>), purchased from VWR and employed without further purification. The polymer employed was Flopaam 3230S (HPAM with MW = 5–8 million Da, 30% hydrolyzed), kindly provided by SNF (France). Model emulsions were prepared with analytical grade hexadecane (Merck, USA) and CTAB surfactant (Sigma-Aldrich, UK). The crude oil originated from the North Sea and was kindly provided by Shell.

## 2.2. Methods

### 2.2.1. Electrodialysis experiments

The electrodialysis experiments were run for 18 h in constant current mode. The current density was fixed at 28.3 A/m<sup>2</sup>, which is 36% of the limiting current density (LCD) when desalting a 53.3 mM NaCl solution. The LCD was experimentally determined through the Cowan and Brown method [25], as described in the [supplementary material](#).

For each experiment, a new membrane, previously conditioned in either NaCl or brackish solution, was placed in the middle compartment of the cell. Once the capillaries were aligned, the experiment was started. The potential over the membrane, pH, and temperature were logged every minute. As soon as the experiment finished, the fluids were removed from the cell and samples were taken. The AEM was removed, dried at room temperature, and stored. Next, the diluate and concentrate solutions were mixed in equal proportions, and the potential between the capillaries was tested for this solution at different currents. This measurement provided the average resistance of the solution, and by combining it with the solution conductivity, the distance  $\delta$  between the capillaries could be calculated [26].

To explore the reversibility of the fouling, some experiments required switching of the direction of the electrical current. By doing so, the solutions in compartments 3 and 4 of the cell were desalted in an alternate form. Each experiment had a specific mineral composition, and made use of solutions with and without HPAM.

### 2.2.2. Membrane analysis

Before being analyzed, the air-dried membranes were frozen in liquid nitrogen and cut using a scalpel. The pieces were stored at room temperature until analyzed. In addition, some membranes were examined by SEM after being freeze-dried. For these samples, a portion of the membrane was cut immediately after the experiment and stored in a freezer at –80 °C. Then, the piece was freeze-dried in a Christ Alpha 2–4 LDplus freeze dryer for 48 h and stored.

**2.2.2.1. SEM/EDX measurements.** The recovered membranes were analyzed with scanning electron microscopy (SEM) and energy-dispersive X-ray spectroscopy (EDX) by JEOL-6480LV (JEOL Ltd. Japan). The samples were gold-coated in a JEOL JFC-1200 fine coater. For SEM, each membrane was examined from three sides:

the two faces and the cross-section. The EDX conditions were 15 kV accelerating voltage and 10 mm working distance.

**2.2.2.2. Raman measurements.** Full Raman spectra (up to 4000 cm<sup>-1</sup>) were obtained by employing a LabRAM HR Raman spectrometer from Horiba Jobin Yvon with an mpc3000 laser at 532.2 nm and a 800 mm focal length achromatic flat field monochromator. The laser was focused through an Olympus Bx41 microscope. The detector was a Synapse multichannel CCD. The spectra taken included both faces of the membranes (focusing on the ion exchange resin and avoiding the supporting fibers), salt precipitates, and a grain of polyacrylamide.

**2.2.2.3. Contact angle measurements.** Static contact angles were measured with a Dataphysics OCA 35 (Germany) contact angle meter by using the sessile drop method (2  $\mu$ l) with MilliQ-water. The droplet was placed on the dry membrane after which a snapshot was taken, and from there the contact angle was determined. The reported values are the average of at least three measurements.

### 2.2.3. Solution analysis

1.5 mL samples of the solutions were taken before and after the experiments and later analyzed for their ionic and carbon species. Cations were measured by using inductive-coupled plasma optical emission spectroscopy (ICP-OES, Optima 5300DV, Perkin Elmer). Anions were analyzed with ion chromatography (IC, 761 Compact IC, Metrohm). The concentration of carbonate species was obtained from the inorganic carbon concentration measured with a TOC analyzer (Shimadzu TOC-VCPH). The particle size distribution of selected HPAM solutions was determined with DIPA 2000 – Particle Analyzer (Prolyse).

## 3. Results and discussion

Section 3.1 combines the analyzes of data logged during the ED and that of the diluate side of the AEMs. Here we show that fouling was observed on both sides of the AEMs, but the effects on electrodialysis performance were mainly attributable to the development of a gel layer on the diluate side. Sections 3.2–3.4 present the analyzes of the concentrate side, process performance, and reversibility. Section 3.5 combines the presented information and literature findings to explain how solution composition affects the fouling by PFPW.

### 3.1. Formation of gel layer by HPAM (diluate side)

A common indication of the formation of a gel layer on a membrane is the increase in electric resistance [13,27]. The changes in resistance were measured as transmembrane electric potential (TMEP) between the two capillaries of our experimental setup. Although the TMEP would be affected by the increase of resistivity of the bulk diluate solution during the experiments, the decrease in conductivity was only 20%, so the impact was minimal. To account for variations among experiments in the distance  $\delta$  between the capillaries, the recorded TMEP was divided by  $\delta$  (Section 2.2.1), and the obtained plots are included as Fig. 2. The results in the Figure are organized to highlight various effects, summarized in Table S1.

**3.1.1. Gel layer in the presence of NaCl and the effect of ionic strength** Fig. 2(A) shows the TMEP development for the experiments E1 to E3. As expected, the TMEP/ $\delta$  of E1, the experiment without foulants, remained constant. In contrast, when HPAM was present in the same solution (E2), there was a clear increase in TMEP. The ini-

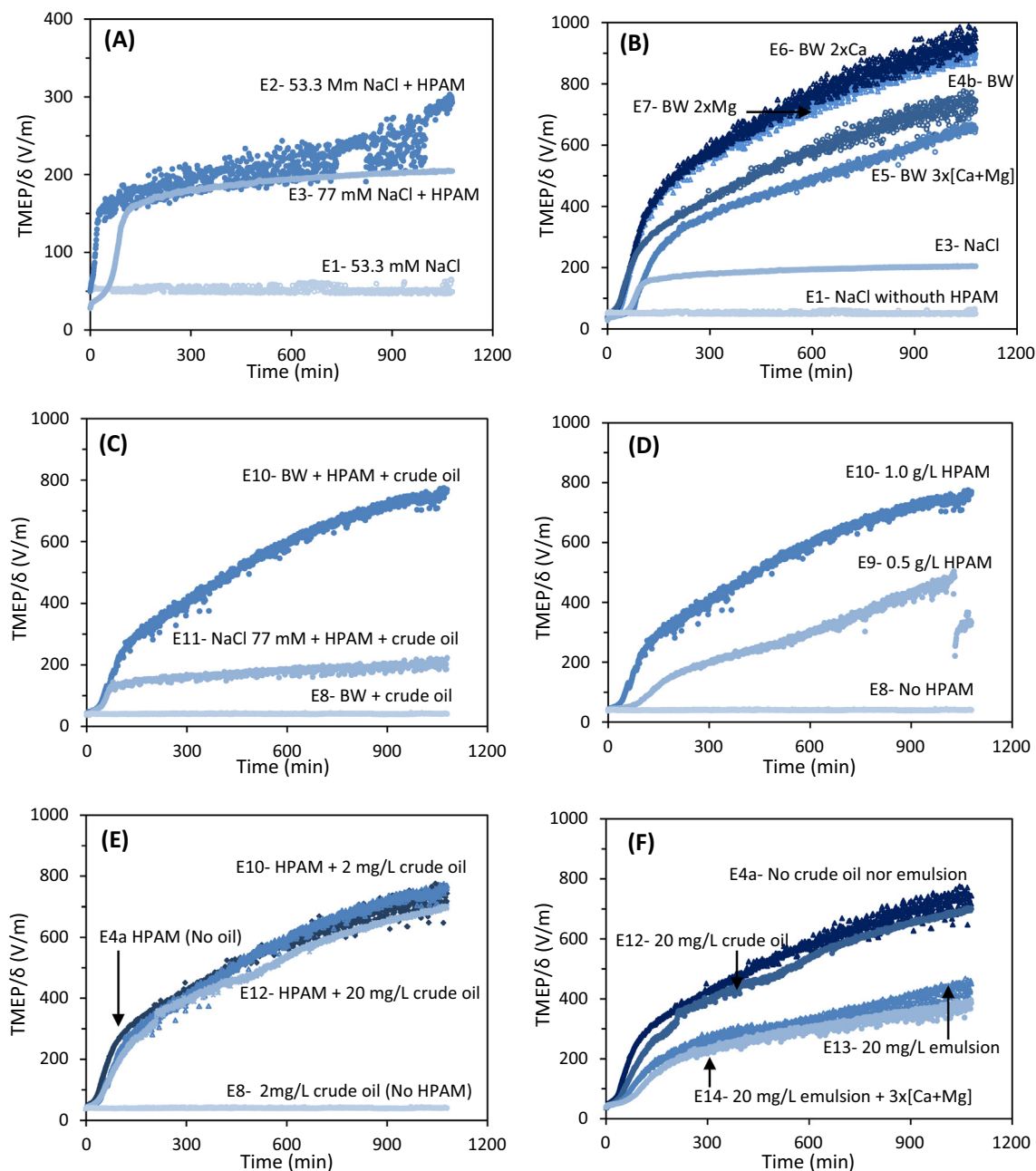


**Fig. 2.** TMEP/δ vs time of ED runs showing assorted effects. (A) Effect of ionic strength and HPAM on TMEP/δ. E1 and E2 had the same ionic strength, while E3 contained a higher concentration of NaCl. (B) Effect of the mineral composition in the absence of oil. (C) Effect of mineral composition in the presence of 2 mg/L of crude oil. (D) Effect of increasing the concentration of HPAM. (E) Effect of the addition of crude oil. (F) Effect of the addition of model emulsion.

tial TMEP/δ of E2 was the same as for E1 because both experiments had the same ionic strength. However, in E2 the potential built up quickly in the first half-hour, after which the increase became more gradual. The periods of instability in the E2 profile could be due to disturbances in the HPAM gel layer or the adhesion of bubbles to the capillaries.

The shape of the TMEP curve is like a typical chronopotentiogram profile [28], with a stabilization time in the order of minutes. The reason for this long stabilizing time is thought to be the slow build-up of the HPAM gel layer. The HPAM layer not only inhibits the replenishment of fresh solution near the membrane, thickening the diffusion boundary layer (DBL), but also causes the ionic transport pathway to become more tortuous [29], all of which increases the electrical resistance, as indicated by the TMEP

profiles. Then, the stabilization period would be reached either when the gel layer stopped growing due to flow conditions in the cell, or when the DBL grew past the capillary tip (so the changes could not be measured anymore). However, the last option is highly unlikely because the reported thicknesses of DBLs are quite below 2.5 mm, which was the approximate distance from the membrane surface to the tip of the capillary. For example, for a 50 mM NaCl solution desalted in a cell without flow, Tanaka reported a DBL of 0.362 mm [30].

The profile of E3 shows two main differences when compared to E2: (i) it originates and stabilizes at a lower TMEP/δ value, and (ii) the voltage increase is less pronounced as it happens during a longer time. Both effects can be attributed to the higher ionic strength of E3. Solutions with higher ionic strength have less resis-

tivity, which explains the lower initial and stabilization values. Additionally, at higher ionic strength the charges of HPAM are more shielded, so the polyelectrolyte becomes effectively less charged. Consequently, the driving force (electrical potential) working on the HPAM has a lower influence, so there is a decrease in polymer migration. This theory contrasts with the one proposed in [17], that suggested that at higher ionic strength, the lower hydrodynamic radius and viscosifying ability would lead to more migration of HPAM towards the anode.

The membranes and their gel layers were further studied with SEM. The Fujifilm type 10 AEM is made of an ion-exchange resin and reinforcement fibers, which are visible on both surfaces and in the cross-section (Fig. 3A). Since the E1 solutions only contained NaCl, no precipitation occurred on the membrane (top row of the figure). The photographs from E2, in the same figure, show a gel layer on the diluate side of the membrane, as expected from the direction of the current in the cell and from the literature [18]. In solution, the polyelectrolyte is negatively charged, so it migrates towards the positively charged electrode (anode) under the influence of the applied voltage, accumulating on the diluate side of the membrane. The gel layer is thin enough to allow to still distinguish the fibers underneath.

The diluate sides of membranes E1 and E2 were also analyzed with Raman. As shown in Fig. 3B, the profile obtained from E2 is closer to that of the dry HPAM granule than to the clean membrane (E1), confirming that the layer on top of the membrane was HPAM.

### 3.1.2. Effect of mineral composition

The effect of mineral composition on the formation of a gel layer can be first examined in Fig. 2B, which shows the  $TMEP/\delta$  for experiments E3 to E7. The most important feature to notice is the continued increase of  $TMEP/\delta$  for the solution with brackish salts (E4b). The slope decreases after the inflection point around minute 100 but does not level off, and the final value is almost four times larger than that of E3 (NaCl + HPAM). The curve for E5 (3x [Ca + Mg]) has the same shape, and although it remains slightly below that of E4b, still reaches a final value three times higher than that of E3. The experiments E6 and E7, with ionic strengths similar to E4 but containing only either calcium or magnesium, presented equally high  $TMEP/\delta$  profiles.

Thereby, two kinds of  $TMEP/\delta$  curves can be distinguished: the ones that tend to flatten relatively early, displayed during the experiments with only NaCl (E2 and E3), and the ones with a continuous increase, which belong to experiments containing a mixed mineral composition (E4 to E7). Indeed, a previous study also reported curves with different slope levels depending on the addition of HPAM of different MW in the solution [15]. In our case, considering that all solutions had approximately the same ionic strength, the observed differences can solely be attributed to the nature of the ions present, and specifically to the presence of divalent cations, as will be further explained in Section 3.5.

The membranes recovered from these experiments were dried in two different ways and analyzed by SEM (Section 2.2.2). As vis-

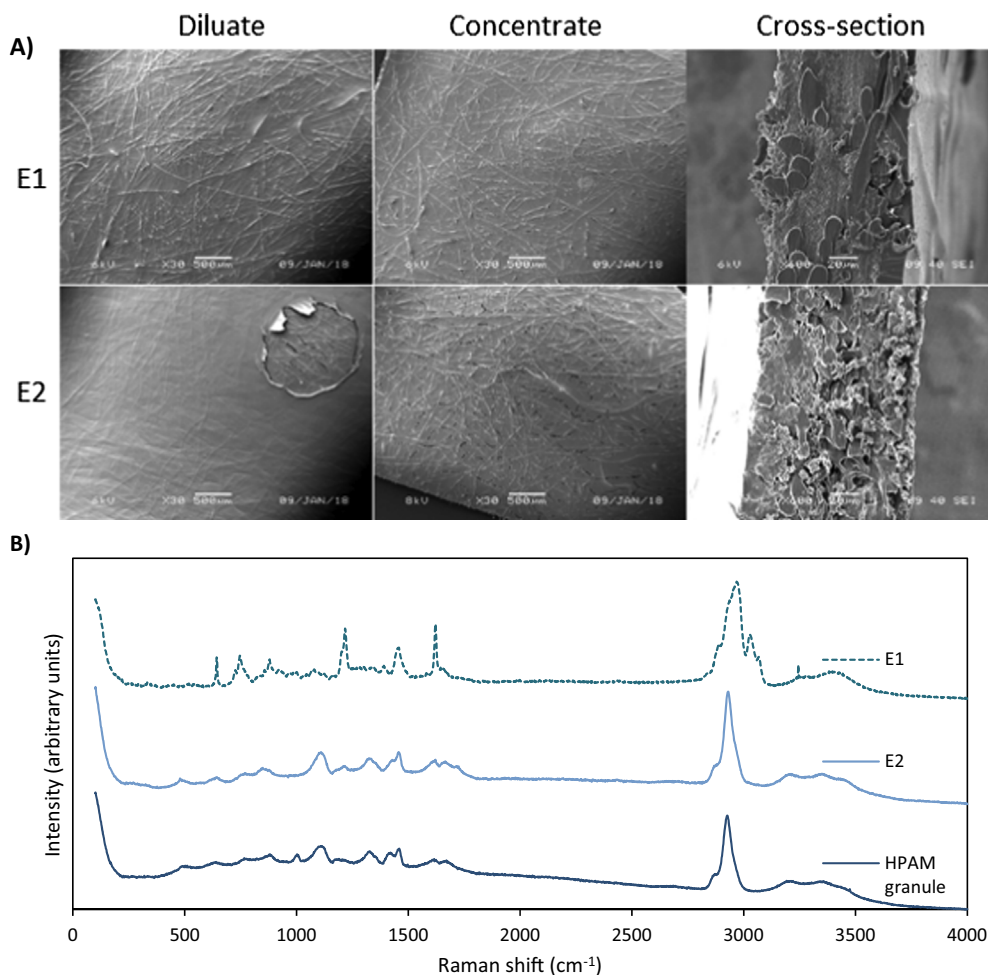


**Fig. 3.** (A) SEM images from membranes E1 (no foulant) and E2 (NaCl + HPAM). The gel layer is visible on the diluate side of E2, but not in the image of the cross-section. (B) Raman profiles from the diluate side of membranes E1 (clean), E2, and a dry HPAM granule.

ible in Fig. 4A, the air-dried gel layers compacted on the surface of the membranes, whereas the freeze-dried membranes maintained some structures, which might still be representative of the morphology of the gel layer as it was during the experiment. Based on the cross-section pictures and EDX analysis (Fig. 4B), the thicknesses of the air-dried gel layers were estimated to be between 5 and 50  $\mu\text{m}$ . In contrast, the freeze-dried layers were significantly thicker, between 50 and 550  $\mu\text{m}$ . The combination of observations, summarized in Table 4, is indicative for the differences in the in situ formation of the gel layer (photos available in Figs. S3 and S4). For example, the freeze-dried layers of the experiments with NaCl solution (E3 and E11) were at least three times smaller than the gel layers from experiments with BW composition. This ratio is very similar to that shown in Fig. 2B, where the final TMEP/ $\delta$  of E4b was approximately 3.5 times larger than that of E3. Thus, our measurements suggest that the differences in the TMEP profiles could have been related to gel layers of different thicknesses, which could be linked to the different mineral compositions in the solutions. This is further discussed in Section 3.5.

The elemental analysis of the diluate side showed differences between the fouled and the clean membranes (Table 5). The AEMs in which a gel layer was visible (E3 to E7) presented a decrease in the percentage of C and an increase in the percentage of N and O,

which corresponds with the composition of the HPAM molecule. Furthermore, the amount of Cl detected diminished when there were thicker gel layers present. As shown in Fig. 4, the ion-exchange resin on the AEM is rich in Cl, so it is logical that when thicker/denser gel layers were formed on top, less Cl from the bottom could be detected.

Raman analyses were also performed on the diluate side of the membranes (data not shown). In all cases, the profiles were very similar to the one of the HPAM granule (Fig. 3B), so this characterization corroborates the gel layer to be formed mainly by HPAM.

### 3.1.3. Effect of mineral composition in the presence of oil

The influence of mineral composition on fouling in the presence of crude oil can be pondered by comparing experiments E8, E10, and E11, which had the same ionic strength and oil content but different mineral composition. Fig. 2C shows that the TMEP/ $\delta$  - time profile of the solution containing only BW plus 2 mg/L of crude oil but without HPAM (E8) remained flat during the whole experiment. The runs with NaCl + HPAM + oil (E11) and with BW + HPAM + oil (E10) showed profiles almost identical to their analogs without oil (E3 and E4a, respectively). As noticed for Fig. 2B, the final TMEP/ $\delta$  value for the experiment containing BW is roughly four times larger than the one containing only NaCl (770

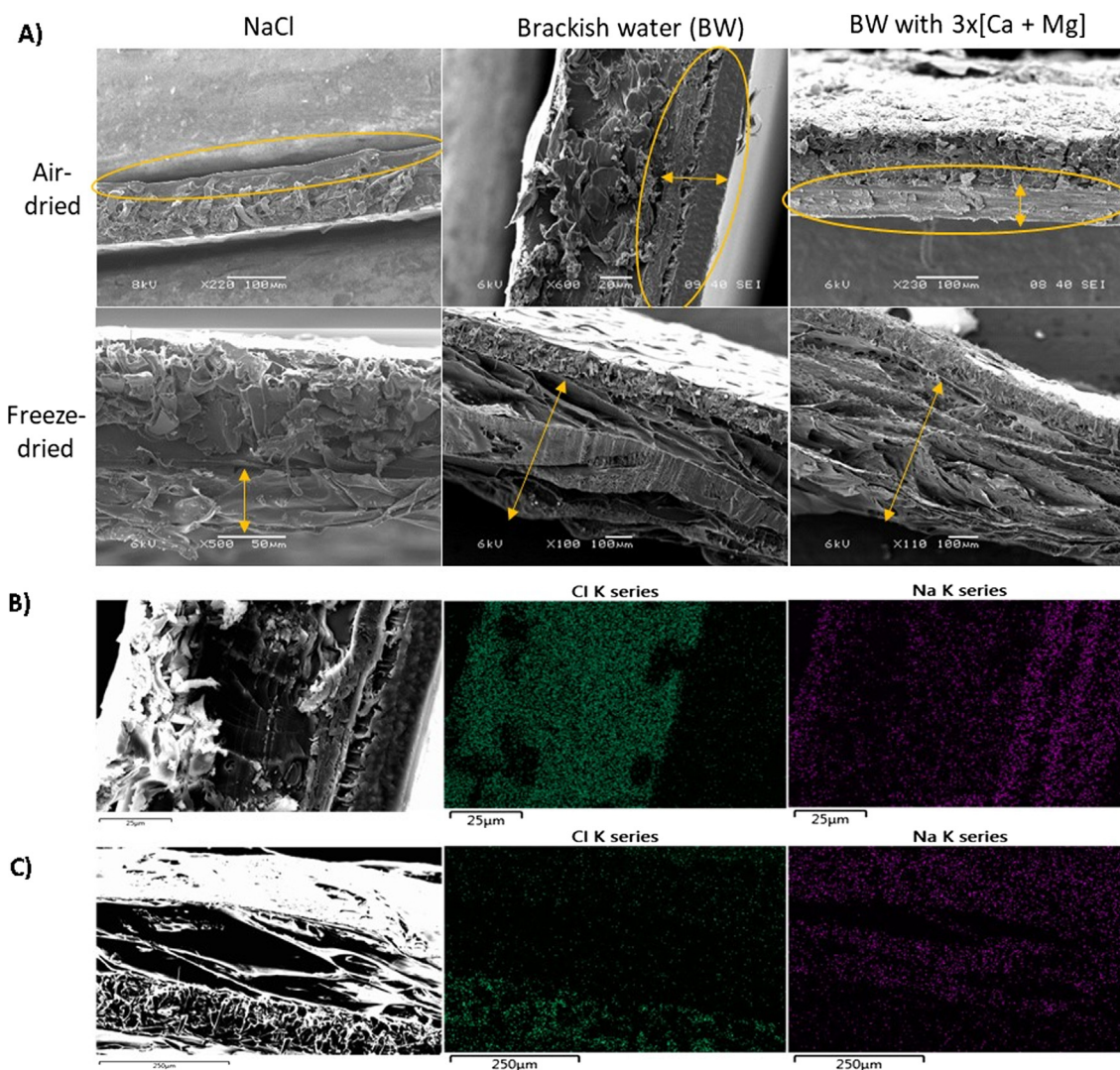


**Fig. 4.** (A) Examples of SEM images of the cross-sections of air-dried and freeze-dried membranes. The arrows and circles indicate the gel layers. (B) EDX analysis of air-dried membrane from E4a. It shows a higher concentration of Cl the ion exchange resin, and Na presence mainly in the HPAM gel layer. (C) EDX images of the freeze-dried membrane of E4b.

**Table 4**  
Summary of the SEM and EDX results.

Membrane	Gel layer thickness (diluate side)			Precipitates (concentrate side) <sup>2</sup>		
	Observed	Air-dried ( $\mu\text{m}$ )	Freeze-dried <sup>1</sup> ( $\mu\text{m}$ )	Type	Common Elements	Traces
1	No	–	–	x	x	FeO, SiO, MgSiO
2	Yes	10	N/A	x	x	SiO
3	Yes	5	50	Scarce crystals	C, O	SO
4a	Yes	34	N/A	Crystals	Ca, O	MgO, MgSiO
4b	Yes	–	500	Crystals	Ca, O	MgO
5	Yes	6	504	Crystals & plaques	Ca, O	MgO
6	Yes	9	355	Crystals & scales	Ca, O	MgO
7	Yes	7	428	Small crystals	Mg, O	–
8	No	–	–	Scarce crystals	Ca, O	MgO
9	Yes	37	N/A	Scarce crystals	Ca, O	NaO
10	Yes	37	N/A	Crystals	Ca, O	MgO
11	Yes	5	120	x	x	NaCl, SiO, FeO
12	Yes	25	N/A	Crystals & plaques	Ca, O	MgO
13	Yes	16	530	x	x	MgSiOAl
14	Yes	52	350	Scales	Ca, O	MgO

<sup>1</sup> N/A indicates that the freeze-drying procedure was not performed for that sample.

<sup>2</sup> The SEM and EDX analysis of the concentrate side was performed on the air-dried membranes.

**Table 5**  
Percentages of the main elements found on the diluate side of membranes E3 to E7.

Element	M1 (Clean)	M3	M4b	M5	M6	M7
<b>C</b>	82.16	52.74	55.78	52.01	56.12	55.60
<b>N</b>	7.27	12.71	17.48	16.59	17.04	16.92
<b>O</b>	4.58	19.90	24.00	24.46	24.44	25.42
<b>Cl</b>	5.82	6.67	0.51	2.18	0.25	0.14
<b>Na</b>	0.02	7.47	1.48	4.14	1.82	1.78

vs 210 V/m). This indicates that the presence of 2 mg/L of crude oil did not have a significant effect on the increase of resistance, which was mostly determined by the mineral composition of the solution and the presence of HPAM.

The membranes recovered from these experiments were also analyzed with SEM and EDX. E8 did not show any significant gel layer nor precipitation. The air-dried membrane from E11 (NaCl), presented a gel layer of approximately 5.0  $\mu\text{m}$ , while the gel layer in E10 (BW) was much thicker (37  $\mu\text{m}$ ) (Table 4). The membrane from E11 was also freeze-dried, and displayed gel layer thickness of 120  $\mu\text{m}$  and a high porosity (Fig. S3). These observations matched with the TMEP profiles, and again showed a correlation between the presence of multivalent ions and the thickness of the HPAM layer.

### 3.1.4. Effect of HPAM concentration

The effect of HPAM concentration in crude oil containing solutions can be evaluated from Fig. 2D. At higher HPAM concentration, there was a higher increase rate of TMEP, as previously reported [18]. However, the membrane analysis indicated gel layers of similar thicknesses for E9 (0.5 g/L HPAM) and E10 (1.0 g/L HPAM). This suggests that the gel layer on E10 was more compact than the one on E9 when assuming no layer materials were lost during recovery. Regarding E8, which did not contain HPAM, no gel layer was observed.

### 3.1.5. Effect of oil addition (crude oil and model emulsion with surfactant)

The effect of increasing the concentration of crude oil can be inferred by comparing experiments E4, E10 and E12. Fig. 2E shows that their TMEP/ $\delta$  - time profiles were alike during most of the experiment, although at the end a slightly lower TMEP/ $\delta$  was recorded for the higher oil concentration (E12). This suggests a destabilization of the gel layer by the oily compounds, limiting its thickness and/or density. This theory is supported by the SEM

observations of the dried gel layer, since membrane E12 had the thinnest of the three experiments (Table 4). Zhang et al. also concluded that the fouling layer formed by HPAM and oil was not as dense as the fouling formed by a single component [6].

Experiments E13 and E14 assessed the effect of an emulsion of hexadecane and CTAB surfactant in the fouling. Comparing these TMEP/ $\delta$  - time profiles with E12 in Fig. 2F, shows that in the presence of 20 mg/L of the hexadecane emulsion the TMEP/ $\delta$  reaches much lower values than when the same concentration of crude oil is added. The destabilizing effect of the emulsion on the HPAM gel layer was larger probably because the positively charged cationic surfactant is attracted towards the (negatively charged) HPAM. Still, the profile of E14 ( $3 \times [\text{Ca} + \text{Mg}]$ ), confirmed that the presence of higher concentrations of divalent cations does not further increase the formation of the gel layer, and it even slows down the increase of TMEP with time, just as observed for E5.

The membranes recovered from E13 and E14 were freeze-dried, and their SEM images revealed well preserved foam-like HPAM layers, thicker than 350  $\mu\text{m}$  (Table 4). The SEM photographs from the diluate side (Fig. S4, 300 X) suggest that the gel layer on E14 was denser than in E13. This observation was reinforced by the EDX analyses of the membranes, which showed that the gel layer in E14 had a higher concentration of C, O, N, and Ca in the upper part (Fig. S5B), indicating a higher concentration of HPAM and possible calcium precipitation. For the rest of the cross-section, the EDX showed that the cations were equally distributed across the gel layer for both E13 and E14.

The most significant difference found between experiments with and without crude oil was the hydrophilicity of the membranes, which was investigated through water contact angle measurements (Section 2.2.2.3). It was found that when a HPAM dried gel layer was present on the diluate side, the contact angle was lower than for the clean membrane, meaning that it made the surfaces more hydrophilic (Fig. S7). On the contrary, when crude oil was present, the hydrophobicity increased, independently of

HPAM being present (E12) or not (E8). These observations coincide with the available literature [13,17], and indicate that hydrophobic oil components interact with both the AEM and the gel layer. Furthermore, Zuo et al. explained that the oil in solution can form negatively charged colloidal structures that migrate towards the diluate side of the AEM [17].

### 3.2. Salt precipitation (concentrate side)

Salt precipitation was found on the concentrate side of most membranes, which is common due to the higher concentration of ions in this compartment. The precipitates were first spotted with SEM, and later analyzed with EDX and Raman. The SEM and EDX results are summarized in Table 4, and Fig. S6 includes the SEM pictures.

SEM allowed to identify three recurrent morphologies for the precipitates, arbitrarily called “crystals”, “scales” and “plaques” (Fig. 5). The precipitation in the form of “crystals” occurred when the solutions had a varied mineral composition, that is, no precipitation was observed for experiments containing only NaCl. The “scales” were large and amorphous precipitates, only observed on the concentrate side of E6 (BW with only Ca) and E14 (BW with  $3\times[\text{Ca} + \text{Mg}]$ ). The “plaques”, which were flat precipitates, appeared when oil was added to the solution. When 2 mg/L of oil was added, the crystals became already more amorphous (E10 in Fig. S6) than when no oil was present. However, the effect amplified significantly with an oil concentration of 20 mg/L (E12), and this membrane presented the highest amount of plaques (Fig. 5C). EDX confirmed that all precipitates had similar compositions (Fig. 5D and E), so the observed differences may be due to the presence of more nucleation sites in which the crystals could start to develop.

In general, more precipitation was observed for experiments that reached higher TMEP/ $\delta$  values due to the presence of HPAM gel layers. For example, the amount of precipitation on membranes

E8 (No HPAM), E9 (0.5 g/L HPAM) and E10 (1.0 g/L HPAM) increased in this order (Fig. S6). The only exception was E7, which presented very few precipitates on the concentrate side. Thus, although the BW experiments with only calcium (E6) and only magnesium (E7) had similar TMEP/ $\delta$  curves and gel layers, they showed contrasting amounts of mineral precipitation (Fig. S5). The differences can be attributed to the slower migration of magnesium and to its higher affinity to the CEM, which reduces its availability on the concentrate stream [31], and to the higher solubility of the magnesium salts compared to the calcium ones.

The EDX analysis indicated that most of the precipitates were composed by Ca and O (Fig. 5D and E), suggesting that they were in the form of calcium carbonate [31–33]. However, this could not be proven via EDX given that the background—the AEM—already had a high carbon content, so any other high concentration of carbon would not stand out. Magnesium was frequently found within the Ca-O precipitates, but in lower concentrations. Other elements detected were K, Na, and Cl, originating from the feed solutions, and others like Si and Fe, which probably originated from impurities in the dissolved salts, polymer, and crude oil.

Raman analysis was also performed on most of the membranes, but it only allowed to identify calcite as one of the precipitates on E14 (Fig. S8). However, considering the EDX results and mentioned literature, it is likely that the precipitates were mainly composed of calcium carbonate.

### 3.3. Performance in terms of the transport of ions

Besides having an effect on the TMEP and in the membrane morphology, fouling is also likely to influence the ion-transport through the membranes and, therefore, the process performance. The transport of anions through the AEM was calculated from the average change in the concentration of anions in the diluate and concentrate compartments. The analysis distinguished between the monovalent ions,  $\text{Cl}^-$  and  $\text{HCO}_3^-$  (considering no pH

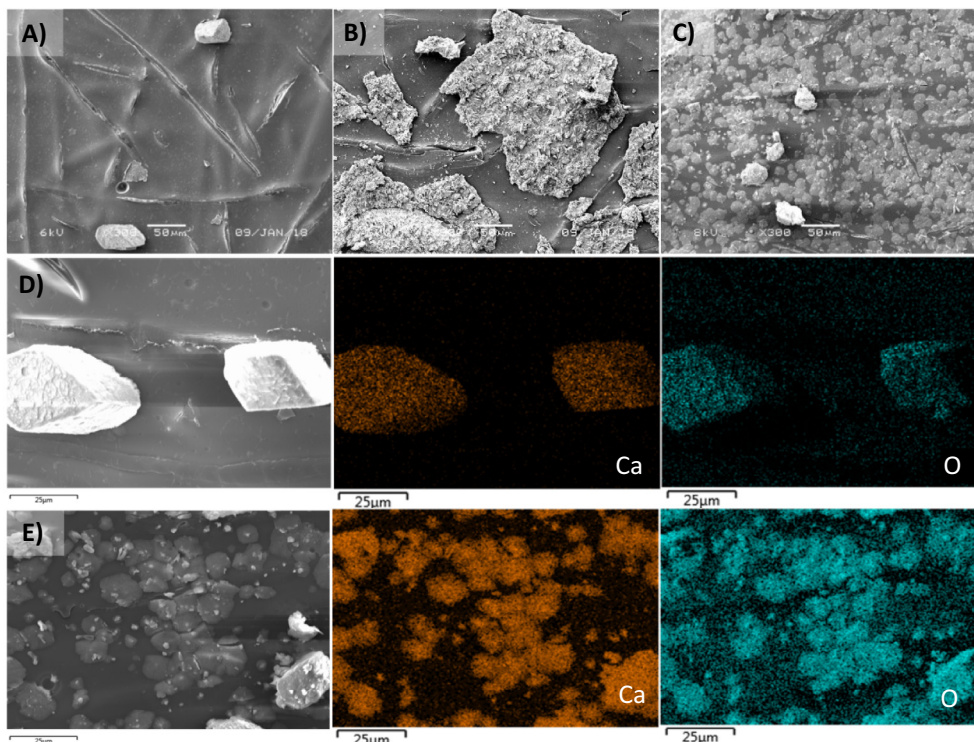


**Fig. 5.** SEM and EDX analysis of precipitates observed on the concentrate side of the AEMs. (A) An example of “crystals”, taken from E4A. (B) Example of “scales” found on E14. (C) Example of “plaques” taken from E12. (D) EDX analysis of precipitates on membrane E4a, including SEM photograph, Ca and O distribution. (E) EDX analysis of precipitates on membrane E12, also showing Ca and O presence.

above 10), and  $\text{SO}_4^{2-}$ , the only divalent anion. The theoretical number of charge equivalents transported (efficiency 100%) was estimated as 13.4 meq (1300 C), calculated from the applied current and the duration of the experiment [2].

Fig. 6 presents the average changes in charge equivalents. In general, the experiments performed reasonably, transporting at least 70% of the theoretical number of equivalents. In most cases, the higher transport of equivalents corresponded to membranes with thinner gel layers. For example, the highest transport of charge equivalents was measured for experiments E11 and E2, which coincide in only having NaCl as mineral composition. On the other hand, the lowest transport was measured for E5 and E14, which presented a thick gel layer and precipitation on the concentrate side due to the extra amount of divalent cations. The comparison of E8, E9, and E10 also shows a better performance when no HPAM was present.

As presented, the decrease in process performance in terms of transport of ions can be related to the incidence of fouling and scaling. The mechanisms behind are the reduction of the permselectivity of the membrane due to the shielding effect of the gel layer, the increase in back-diffusion of ions, and the occurrence of water splitting [29]. The latter phenomenon was further analyzed through pH measurements, which demonstrated significant quantities of water splitting, as further explained in the [Supplementary Material](#).

### 3.4. Reversibility of fouling

The reversibility of the fouling was assessed through electrodiagnosis reversal experiments, each performed either with NaCl or BW composition. We present first the analysis for the NaCl experiment (Fig. 7A). Before applying the electric current in a certain direction, the open-circuit voltage (OCV) of the cell was recorded. Since the cell might have some asymmetry, comparisons are made among periods with the same current direction. For the first two periods of 30 min, compartments 3 and 4 contained NaCl solutions without HPAM. As expected since there were no foulants, the  $\text{TMEP}/\delta$  values were constant, independently of the direction of the current. Then, after adding the solution with 1.0 g/L of HPAM (1 in the plot), the  $\text{TMEP}/\delta$  curve increased in a sinusoidal shape, as observed in previous experiments, indicating the build-up of the gel layer. The current direction was maintained for 60 min, allowing the formation of a HPAM layer, and then reversed at minute 125. After the reversal, the  $\text{TMEP}/\delta$  stabilized at the original value of  $-55$  V/m, but when the current was reversed again to the positive direction (minute 160), the  $\text{TMEP}/\delta$  increased again. Then, at point 2, the solution with HPAM is substituted by a solution without foulant, which causes a decrease in the TMEP, although it does not reach the base

value. Finally, the  $\text{TMEP}/\delta$  values during the last 30 min of the experiment were closer to the initial ones. A similar behavior was observed for the experiment with BW (Fig. 7B), with the main difference that when the foulant was added, the increase in TMEP was much faster, as in previous experiments.

There are some details to highlight. The fact that after reversing the current at minute 125 the TMEP goes back to its original value, indicates that the fouling only has a tangible effect when it coincides with the diluate side of the membrane. This confirms that the increase in TMEP is caused by the depletion of ions at the diluate side of the AEM due to concentration polarization [34]. The HPAM layer is still present when the current stopped at minute 125, as indicated by the higher OCV value. Thus, when the current is reversed, the HPAM layer is probably still interacting with the membrane, but its effect is minimal since now it is placed on the concentrate side.

It is also noteworthy that the formation of the second HPAM layer (minute 160), goes slightly faster than the first time that a layer was formed. This can be interpreted as a partial removal of the gel layer by the current reversal. However, when the solution without foulant is added and the current is reversed once more, the initial TMEP values are recovered. Two reasons could explain that the solution without HPAM has better results in removing the gel layer: (i) the concentration gradient between the gel layer and the fresh solution, and (ii) turbulence. The latter arises from the lower viscosity of the solution without HPAM [2], which causes more turbulence in the cell and therefore higher shear forces that overcome the remaining attraction of the fouling layer towards the membrane.

Thus, our experiments indicate that the HPAM gel layer, or at least most part of it, can be removed by a combination of current reversal and use of clean solutions. However, this is not a definite conclusion, as will be further explained in the following section.

### 3.5. General fouling mechanism

Once the results from the membrane analyses have been presented, this section combines the observations from the experiments into a fouling model.

#### 3.5.1. Distinction between adsorption of polyelectrolyte and formation of a gel-layer

First of all, we would like to distinguish between two mechanisms involved in the fouling of AEMs by HPAM: (i) the adsorption of the polyelectrolyte on the surface of the AEM, and (ii) the development of a gel layer due to transport of HPAM towards the membrane and the entanglement of the polymer chains [18]. Indeed,

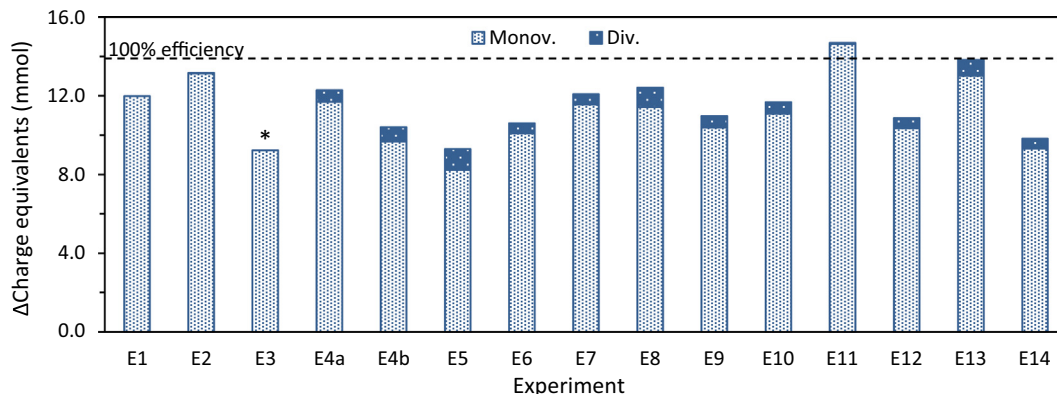
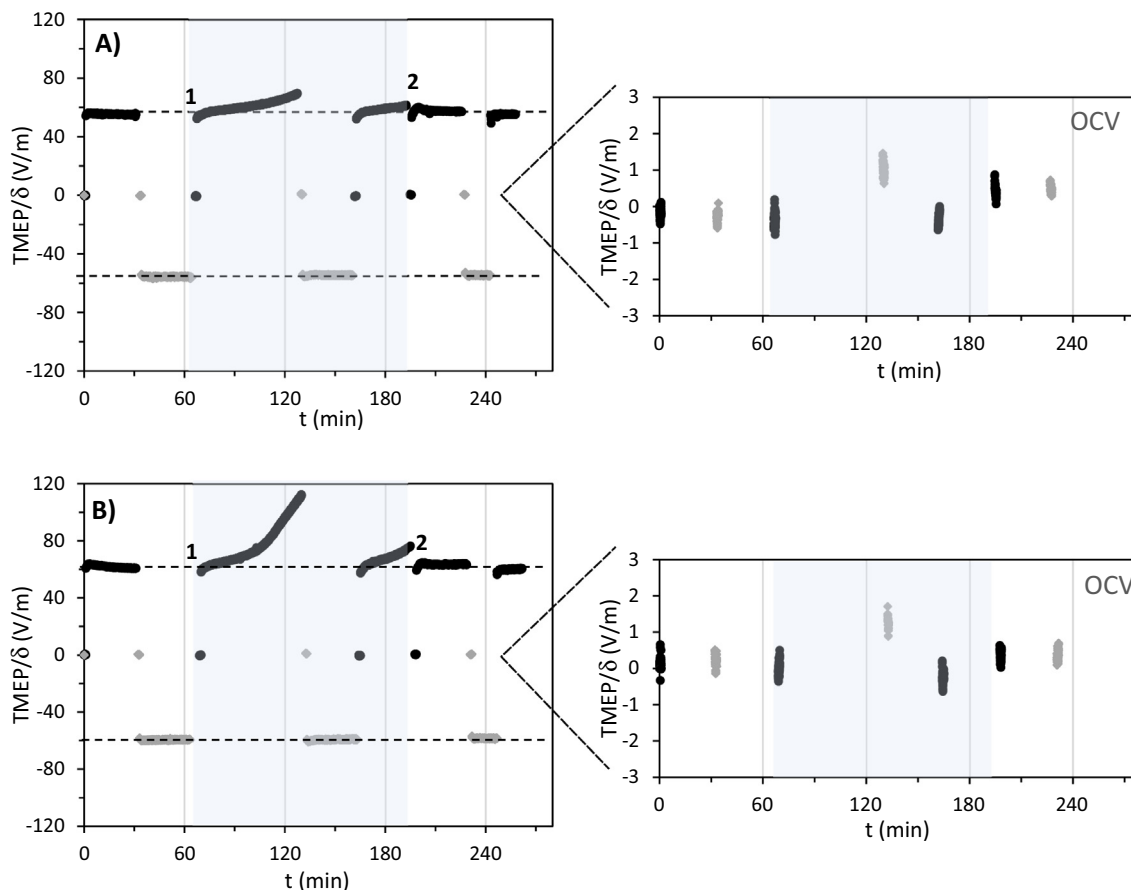


Fig. 6. Average change of monovalent and divalent anions, presented as charge equivalents, in the diluate and concentrate solutions. The theoretical change in equivalents given the applied current and operative time was 13.4 meq, indicated by the discontinuous line (100% efficiency). The low performance measured in E3 can be attributed to a leaking capillary, detected after running the experiment. The traces of sulfate detected in E2 and E11 probably originated from the electrode compartments.



**Fig. 7.** TMEP/ $\delta$  profile for the current reversal experiment with (A) NaCl solution and, (B) BW solution. Initially, the compartments 3 and 4 contained solutions without foulants. At point 1, the solution on the diluate side was switched for a solution with the same mineral composition but containing 1 g/L of HPAM. At point 2, the solution with HPAM is substituted by the solution without foulant. Thus, the shaded area indicates when the solution with HPAM was present in the cell. The plots at the right are included to highlight the OCV measurements, which tended towards zero.

when studying organic fouling on other types of polymeric membranes, authors have used a similar approach, differentiating between membrane-foulant and foulant-foulant interactions [35,36].

Regarding the adsorption stage, it has been thoroughly described how polyelectrolytes, including hydrolyzed polyacrylamide, adsorb on (oppositely charged) surfaces [37–40]. The adsorption occurs even when the concentration of polyelectrolyte in solution is as low as 1.0 mg/L, and is usually considered irreversible [39]. In contrast, a gel layer needs higher concentrations to develop, and since it would be physically attached, it should be reversible. This distinction between two mechanisms also helps to explain the results from Section 3.4, which confirmed that most part of the gel layer was dispersed, but gave no evidence of the adsorbed layer. Actually, the literature suggests that the increase in resistance of a membrane with an adsorbed layer of polyelectrolyte would be minimal [41], and non-detectable with the current method, as observed in preliminary experiments (Fig. S10). Thus, to confirm if adsorbed HPAM remains on the AEM after applying current reversal, other techniques would need to be employed.

However, for the relatively high concentration of HPAM in the PFPW of this study, the main fouling process is thought to be agglomeration near the membrane surface. During the electro dialysis, this anionic polyelectrolyte migrates towards the anode and accumulates on the diluate side of the AEM. The HPAM tends to accumulate predominantly due to the electrostatic attraction that exists between the charged polymer and AEM [17], and the van der Waals attraction that exists between polymer and membrane

materials. Due to the increasing concentration of polyelectrolyte, the local viscosity of the solution also increases [17], creating a gel layer that can stay in place under moderate shear rates. Even when the surrounding solution is removed, the high viscosity of the gel layer retards the water depletion out of the gel layer, keeping the polymer–polymer and polymer–surface interactions intact and the gel layer due to that at its place, close to the AEM, so when the membrane is recovered the gel layer comes together with it.

### 3.5.2. Ionic strength of solution and divalent cations influence the fouling by HPAM

There are at least two aspects of the solution composition that directly affect the fouling by HPAM: the ionic strength and the presence of divalent cations. The ionic strength impacts the migration of HPAM towards the membrane, as suggested by the delayed and lower TMEP/ $\delta$  profiles of the experiments with higher ionic strength. Regarding the divalent cations (calcium and magnesium), it was found that they affect the formation and morphology of the HPAM gel layer. Experiments with brackish composition reached TMEP values 3–5 times higher than for experiments in which only NaCl was present. These observations can be explained in that the divalent cations complexate HPAM molecules by forming inter and intra molecular bridges between them [6,20]. The complexation starts when HPAM and divalent cations are put in contact in the solution, but can continue for hours [20], thus it keeps occurring while the gel layer is forming. In specific, we found in the literature four phenomena related to the complexing effect of divalent cations that could have an effect on the formation of the gel layer;

one related to the membrane-foulant interaction and three to the foulant-foulant interaction.

Concerning the membrane-foulant interaction, it has been documented that when divalent cations are in solution, more mass of polyelectrolyte can be adsorbed than when only monovalents are present [40,42]. Depending on the concentration of divalent cations, polyelectrolyte chains can form micelles and thus would adsorb as aggregated molecules [40], which increases the amount of matter per area unit. The formation of aggregates and the coiling up of HPAM molecules also explains the first phenomenon related to the foulant-foulant interaction, which is that the gel layer formed in the presence of divalent cations can be more compact and denser [6]. We performed particle size analyses on HPAM solutions in NaCl, BW, and BW with  $3x[Ca + Mg]$  and found, respectively, average sizes of 7.89, 7.37 and 5.33  $\mu\text{m}$ . This means that the size of the particles decreased as the concentration of divalent cations increased, in agreement with previous measurements done for polyacrylamide solutions [43]. The second effect of divalent cations regarding the foulant-foulant interaction is that they could cause stronger adhesion forces between carboxylate-containing molecules (like HPAM), as reported in [35] for a fouled membrane and a probe with carboxylate groups on its surface. The third factor is that gels formed by polyacrylamide and divalent cations are reported to shrink with time [44]. A fourth factor, not particularly related to the presence of divalent cations but to the high voltages reached in the cell when they were present, is that HPAM gels can also diminish their volume under the influence of electric fields [45].

The aforementioned factors suggest that the gel layers formed in the presence of divalent cations are more compact and resistant to shear forces than the gels containing only monovalent cations. Indeed, the SEM images of some freeze-dried membranes support this theory (Fig. 8). For solutions with BW composition, the continuous increase of the TMEP profiles even past the inflection point could mean that the gel layer was increasing in thickness and/or density thanks to the morphology given by the divalent cations.

Regarding the effect of the crude oil, it is suggested that it acts as a destabilizer of the HPAM-gel layers, as indicated by the slightly lower TMEP profiles and thinner gel layer thicknesses obtained when present in the feed solution. It can be that some charged oil components migrate towards the anode [17] and get embedded in the gel-layer, becoming impurities that make the layer less resistant to shear forces. Nevertheless, the employed oil concentrations were small compared to that of HPAM, so the observed effects were minimal.

### 3.5.3. Effects of the HPAM gel layer

The formation of the gel layer would have limited the replenishment of ions from the bulk solution to the surface of the AEM (concentration polarization), increasing the thickness of the diffusion boundary layer and causing the decrease of anions' concentration on the diluate side of the AEM. Due to the low concentration of anions, water eventually started to dissociate on the diluate side of the AEM, producing protons and hydroxyl groups [34]. This is exemplified in Fig. 9, which shows that the pH changes started to

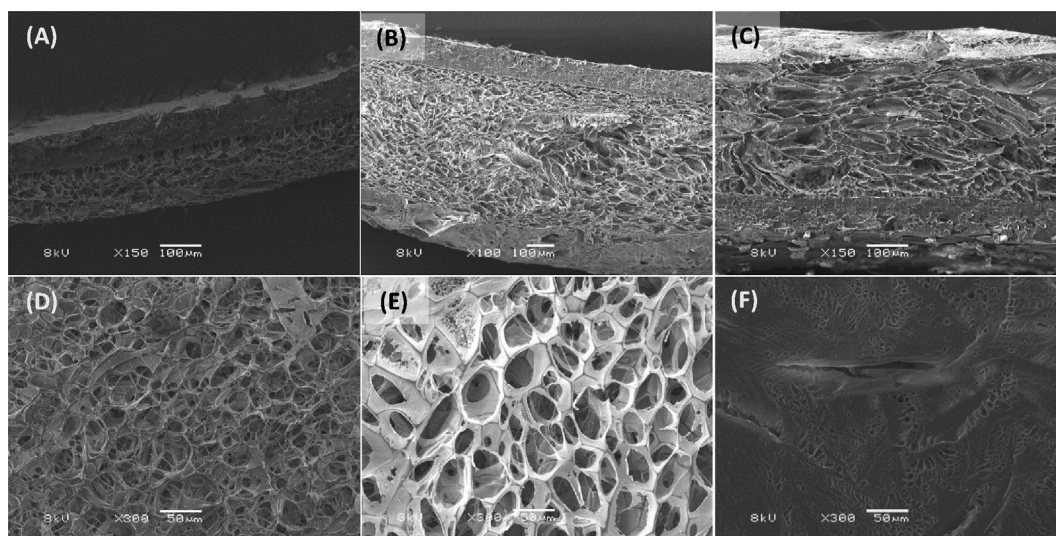


**Fig. 8.** Selected SEM images that illustrate the influence of divalent cations on HPAM layer thickness and density. Images (A), (B) and (C) show, respectively, the cross-sections of E11 (NaCl 77 mM), E13 (BW) and E14 (BW with triple divalent cations). Images (D), (E) and (F) show the top view of the same membranes in the mentioned order.

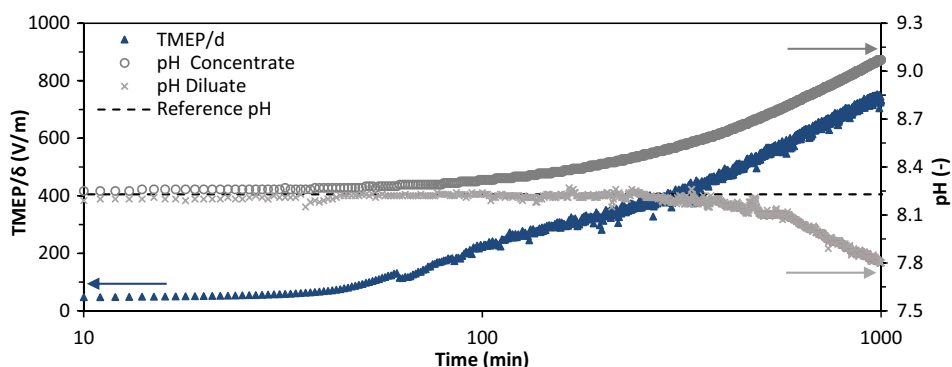


**Fig. 9.** TMEP/ $\delta$ , pH of the diluate and pH of the concentrate during E10. The discontinuous line is plotted as a reference for the pH.

occur soon after the TMEP started to increase, and they continue during the rest of the experiment. The protons tend to go towards the cathode, but first must go through the HPAM gel layer, where some of them might get adsorbed. This could have two consequences: a slight reduction of the coil size (the HPAM in the gel layer is in the overlap regime, so the coils have already their random coil size), and the neutralization of the HPAM gel layer on the AEM [29]. Still, the pH on the diluate stream decreases, which can enhance HPAM precipitation [46] and, consequently, the constraints for the transport of ions, which translates in an autocatalytic or self-amplifying process [34].

Salt precipitation on the concentrate side of the AEM is also linked to the presence of the gel layer. While the HPAM layer is forming, water dissociation occurs at the interface of the layer and the AEM. The hydroxide ions migrate towards the concentrate side of the AEM, where two events can take place: (i) divalent cations can precipitate directly with the hydroxide, and (ii) the pH increases, allowing bicarbonate to be converted to carbonate, which can also increase precipitation [31]. The gel layer-precipitation relationship was demonstrated in E8 (no gel layer and minimal precipitation) and E9 (less HPAM in solution leading to slight precipitation).

#### 4. Conclusions

In the applied concentration range, HPAM is the dominant foulant in terms of resistance increase and coverage of the AEM. Its anionic charge causes it to migrate towards the surface of the membrane at the diluate side when the electrical current is applied. There are two fouling mechanisms for the HPAM on the AEM: (i) it adsorbs to the oppositely charged membrane due to electrostatic and hydrophobic interactions [18], and (ii) it concentrates near the membrane surface and forms a gel layer of polyelectrolyte. However, most of the effects analyzed in this study are attributable to the formation of the gel layer on the diluate side of the membrane.

The mineral composition of polymer-flooding produced water influences the thickness and structure of the HPAM gel layer. Increased ionic strength decreases the migration of HPAM by coverage of negative charges. The presence of divalent cations in the solution likely causes the formation of thicker and denser HPAM gel layers. The presence of these gel layers hampers the replenishment of ions from the bulk solution to the surface of the membrane, lowering the limiting current density of the system. This condition triggers local pH changes and the precipitation of salts on the concentrate side of the AEM.

Despite its mineral composition, the gel layer shows a reversible nature when a combination of current reversal and foulant-free solution is employed, but most likely the small HPAM amount that is adsorbed on the surface of the AEM remains there, but barely affects the membrane performance.

Salt precipitation occurred frequently on the concentrate side of the membranes, mostly in the form of calcium carbonate. The presence of crude oil changed the morphology of the calcium carbonate precipitation and was found to destabilize the HPAM gel layer.

Our results agree with Xia et al. [13] regarding the joint effect of HPAM plus mineral foulants, but differ from theirs concerning the impact of the crude oil and oily compounds. For the present study, the effect of crude oil, either alone or in combination with the rest of the foulants, was minimal. The difference might be due to (1) the lower oil concentration used in the present study, (2) the variable properties of crude oil depending on its origin [47], and (3) the use of membranes based on different chemistries. While the Fujifilm AEMs employed in the present study are based in an aliphatic compound (acrylamide), the membranes used by Xia et al. were based

on an aromatic one (polyphenylene) [13]. Previous studies have indicated that membranes based on aliphatic compounds are less prone to suffer from organic fouling [48–50]. It is understood that the aromatic fractions of crude oil have a higher affinity for aromatic composed membranes, and thus have a high tendency to adsorb on them (i.e. through  $\pi$ - $\pi$  interactions). Alternatively, aliphatic oil fractions predominantly adsorb on membranes through hydrophobic interactions, and the ab- and adsorbed layers appear to have only a minor effect on the functioning of the membranes used in our study. Thus, it appears that aliphatic membranes are also more suitable to treat streams containing crude oil, despite it naturally consists of a mixture of aliphatic and aromatic compounds.

If the TMEP values recorded during the experiments are converted to resistances (using Ohm's law), some of them are above  $900 \Omega \cdot \text{cm}^2$ , which are notoriously high for a membrane and the liquid adjacent to it. Indeed, in our previous research employing a membrane stack [2], such high resistances were never reached. The thick gel layers and consequent high resistances might have been propitiated by the hydrodynamic conditions in the six-compartment cell, which has thick compartments and lacks spacers to increase the turbulence. In order to better quantify the effect of fouling, it would be ideal to have flow conditions which are closer to the ones in an ED stack.

#### Acknowledgments

This work was performed in the cooperation framework of Wetsus, European Centre of Excellence for Sustainable Water Technology ([www.wetsus.nl](http://www.wetsus.nl)). Wetsus is co-funded by the Dutch Ministry of Economic Affairs and Ministry of Infrastructure and Environment, the European Union Regional Development Fund, the Province of Fryslân, and the Northern Netherlands Provinces. This research has received funding from the European Union's Horizon 2020 research and innovation programme under the Marie Skłodowska-Curie grant agreement No 665874. We are grateful to the participants of the research theme "Desalination" for fruitful discussions and financial support. The authors also would like to thank Mr. Diego Pintossi for his aid programming the experimental protocol in the Autolab software, as well as to Mr. David Lewis for the English language correction of the manuscript.

#### Appendix A. Supplementary material

Supplementary data to this article can be found online at <https://doi.org/10.1016/j.jcis.2019.09.029>.

#### References

- [1] S. Liu, D.O. Company, X. Dong, H. Ban, T. Wang, W. Pan, Technology for Confacting Polymer Solution with Desalinated Produced Water. Paper SPE 110237, in: SPE (Ed.), 2007 SPE Annu. Tech. Conf. Exhib. Anaheim, California, USA, SPE, Richardson, TX, 2007: pp. 1–5.
- [2] P.A. Sosa-Fernandez, J.W. Post, H. Bruning, F.A.M. Leermakers, H.H.M. Rijnaarts, Electrodialysis-based desalination and reuse of sea and brackish polymer-flooding produced water, *Desalination* 447 (2018) 120–132, <https://doi.org/10.1016/j.desal.2018.09.012>.
- [3] D.C. Standnes, I. Skjevraak, Literature review of implemented polymer field projects, *J. Pet. Sci. Eng.* 122 (2014) 761–775, <https://doi.org/10.1016/j.petrol.2014.08.024>.
- [4] J.J. Sheng, B. Leonhardt, N. Azri, Status of Polymer-Flooding Technology, *J. Can. Pet. Technol.* 54 (2015) 116–126, <https://doi.org/10.2118/174541-PA>.
- [5] J.A. Herschell, Water and wastewater treatment for enhanced oil recovery, Mahon, Cork, Ireland, 2016.
- [6] R. Zhang, W. Shi, S. Yu, W. Wang, Z. Zhang, B. Zhang, L. Li, X. Bao, Influence of salts, anion polyacrylamide and crude oil on nanofiltration membrane fouling during desalination process of polymer flooding produced water, *Desalination*. 373 (2015) 27–37, <https://doi.org/10.1016/j.desal.2015.07.006>.
- [7] G. Jing, L. Xing, S. Li, C. Han, Reclaiming polymer-flooding produced water for beneficial use: Salt removal via electrodialysis, *Desalin. Water Treat.* 25 (2011) 71–77, <https://doi.org/10.5004/dwt.2011.1766>.

- [8] L. Henthorne, G.A. Pope, U. Weerasooriya, V. Llano, Impact of Water Softening on Chemical Enhanced Oil Recovery, in: Proc. - SPE Symp. Improv. Oil Recover. 2014, SPE, Tulsa, Oklahoma, 2014.
- [9] B. Sparrow, A. Ebsary, D. Mandel, M. Man, An advanced electrochemical system for EOR produced water desalination and reduced polymer consumption, in: Proc. - SPE Symp. Improv. Oil Recover. 2018, SPE, Tulsa, Oklahoma, 2018.
- [10] J. Guolin, W. Xiaoyu, H. Chunjie, The effect of oilfield polymer-flooding wastewater on anion-exchange membrane performance, Desalination. 220 (2008) 386–393, <https://doi.org/10.1016/j.desal.2007.03.010>.
- [11] J. Guolin, X. Lijie, L. Yang, D. Wenting, H. Chunjie, Development of a four-grade and four-segment electro dialysis setup for desalination of polymer-flooding produced water, Desalination. 264 (2010) 214–219, <https://doi.org/10.1016/j.desal.2010.06.042>.
- [12] S. Mikhaylin, L. Bazinet, Fouling on ion-exchange membranes: Classification, characterization and strategies of prevention and control, Adv. Colloid Interface Sci. 229 (2016) 34–56, <https://doi.org/10.1016/j.cis.2015.12.006>.
- [13] Q. Xia, H. Guo, Y. Ye, S. Yu, L. Li, Q. Li, R. Zhang, Study on the fouling mechanism and cleaning method in the treatment of polymer flooding produced water with ion exchange membranes, RSC Adv. 8 (2018) 29947–29957, <https://doi.org/10.1039/c8ra05575k>.
- [14] H. Guo, F. You, S. Yu, L. Li, D. Zhao, Mechanisms of chemical cleaning of ion exchange membranes: A case study of plant-scale electro dialysis for oily wastewater treatment, J. Memb. Sci. 496 (2015) 310–317, <https://doi.org/10.1016/j.memsci.2015.09.005>.
- [15] T. Wang, S. Yu, L. an Hou, Impacts of HPAM molecular weights on desalination performance of ion exchange membranes and fouling mechanism, Desalination 404 (2017) 50–58, <https://doi.org/10.1016/j.desal.2016.10.007>.
- [16] J.L.S. Aguiar, C.R.E. Mansur, The influence of polymer flooding on produced oily water: a review, Brazilian J. Pet. Gas. 10 (2016) 49–61, <https://doi.org/10.5419/bjppg2016-0005>.
- [17] X. Zuo, L. Wang, J. He, Z. Li, S. Yu, SEM-EDX studies of SiO<sub>2</sub>/PVDF membranes fouling in electro dialysis of polymer-flooding produced wastewater: Diatomite, APAM, and crude oil, Desalination 347 (2014) 43–51, <https://doi.org/10.1016/j.desal.2014.05.020>.
- [18] H. Guo, L. Xiao, S. Yu, H. Yang, J. Hu, G. Liu, Y. Tang, Analysis of anion exchange membrane fouling mechanism caused by anion polyacrylamide in electro dialysis, Desalination 346 (2014) 46–53, <https://doi.org/10.1016/j.desal.2014.05.010>.
- [19] P.A. Sosa-Fernandez, J.W. Post, F.A.M. Leermakers, H.H.M. Rijnaarts, H. Bruning, Removal of divalent ions from viscous polymer-flooding produced water and seawater via electro dialysis, J. Memb. Sci. 589 (2019) 117251, <https://doi.org/10.1016/j.memsci.2019.117251>.
- [20] S. Peng, C. Wu, Light scattering study of the formation and structure of partially hydrolyzed poly(acrylamide)/calcium(II) complexes, Macromolecules 32 (1999) 585–589.
- [21] P. Dugolecki, K. Nymejier, S. Metz, M. Wessling, Current status of ion exchange membranes for power generation from salinity gradients, J. Memb. Sci. 319 (2008) 214–222, <https://doi.org/10.1016/j.memsci.2008.03.037>.
- [22] B. Van Berchum, W.J. Van Baak, J. Hessing, Curable compositions and membranes, US 9,309,343 B2, 2016.
- [23] A.R. Al-Hashmi, T. Divers, R.S. Al-Maamari, C. Favero, A. Thomas, Improving polymer flooding efficiency in Oman oil fields. Paper SPE-179834-MS, in: SPE EOR Conf. Oil Gas West Asia Held Muscat, Oman, 21–23 March 2016., SPE, Muscat, 2016: p. 18.
- [24] J.M. Dickhout, J.M. Kleijn, R.G.H. Lammertink, W.M. de Vos, Adhesion of emulsified oil droplets to hydrophilic and hydrophobic surfaces – effect of surfactant charge, surfactant concentration and ionic strength, Soft Matter. 14 (2018) 5452–5460, <https://doi.org/10.1039/C8SM00476E>.
- [25] D.A. Cowan, J.H. Brown, Effect of turbulence on limiting current in electro dialysis cells, Ind. Eng. Chem. 51 (1959) 1445–1448, <https://doi.org/10.1021/ie50600a026>.
- [26] P. Sistat, A. Kozmai, N. Pismenskaya, C. Larchet, G. Pourcelly, V. Nikonenko, Low-frequency impedance of an ion-exchange membrane system, Electrochim. Acta. 53 (2008) 6380–6390, <https://doi.org/10.1016/j.electacta.2008.04.041>.
- [27] H.J. Lee, S.H. Moon, S.P. Tsai, Effects of pulsed electric fields on membrane fouling in electro dialysis of NaCl solution containing humate, Sep. Purif. Technol. 27 (2002) 89–95, [https://doi.org/10.1016/S1383-5866\(01\)00167-8](https://doi.org/10.1016/S1383-5866(01)00167-8).
- [28] N. Pismenskaia, P. Sistat, P. Huguet, V. Nikonenko, G. Pourcelly, Chronopotentiometry applied to the study of ion transfer through anion exchange membranes, J. Memb. Sci. 228 (2004) 65–76, <https://doi.org/10.1016/j.memsci.2003.09.012>.
- [29] J.S. Park, J.H. Choi, K.H. Yeon, S.H. Moon, An approach to fouling characterization of an ion-exchange membrane using current-voltage relation and electrical impedance spectroscopy, J. Colloid Interface Sci. 294 (2006) 129–138, <https://doi.org/10.1016/j.jcis.2005.07.016>.
- [30] Y. Tanaka, Concentration polarization in ion-exchange membrane electro dialysis: the events arising in an unforced flowing solution in a desalting cell, J. Memb. Sci. 244 (2004) 1–16, <https://doi.org/10.1016/j.memsci.2004.02.041>.
- [31] N. Cifuentes-Araya, C. Astudillo-Castro, L. Bazinet, Mechanisms of mineral membrane fouling growth modulated by pulsed modes of current during electro dialysis: evidences of water splitting implications in the appearance of the amorphous phases of magnesium hydroxide and calcium carbonate, J. Colloid Interface Sci. 426 (2014) 221–234, <https://doi.org/10.1016/j.jcis.2014.03.054>.
- [32] N. Cifuentes-Araya, G. Pourcelly, L. Bazinet, Water splitting proton-barriers for mineral membrane fouling control and their optimization by accurate pulsed modes of electro dialysis, J. Memb. Sci. 447 (2013) 433–441, <https://doi.org/10.1016/j.memsci.2013.06.055>.
- [33] C. Casademont, G. Pourcelly, L. Bazinet, Effect of magnesium/calcium ratios in solutions treated by electro dialysis: Morphological characterization and identification of anion-exchange membrane fouling, J. Colloid Interface Sci. 322 (2008) 215–223, <https://doi.org/10.1016/j.jcis.2008.02.068>.
- [34] E. Korngold, F. de Korosy, R. Rahav, M.F. Taboch, Fouling of anionselective membranes in electro dialysis, Desalination 8 (1970) 195–220, [https://doi.org/10.1016/S0011-9164\(00\)80230-1](https://doi.org/10.1016/S0011-9164(00)80230-1).
- [35] Q. Li, M. Elimelech, Organic fouling and chemical cleaning of nanofiltration membranes: Measurements and mechanisms, Environ. Sci. Technol. 38 (2004) 4683–4693, <https://doi.org/10.1021/es0354162>.
- [36] X. Jin, X. Huang, E.M.V. Hoek, Role of specific ion interactions in seawater RO membrane fouling by alginic acid, Environ. Sci. Technol. 43 (2009) 3580–3587, <https://doi.org/10.1021/es8036498>.
- [37] I. Szilagyi, G. Trefalt, A. Tiraferri, P. Maroni, M. Borkovec, Polyelectrolyte adsorption, interparticle forces, and colloidal aggregation, Soft Matter. 10 (2014) 2479–2502, <https://doi.org/10.1039/c3sm52132j>.
- [38] E. Pefferkorn, Polyacrylamide at solid/liquid interfaces, J. Colloid Interface Sci. 216 (1999) 197–220.
- [39] M. Porus, P. Maroni, M. Borkovec, Structure of adsorbed polyelectrolyte monolayers investigated by combining optical reflectometry and piezoelectric techniques, Langmuir. 28 (2012) 5642–5651, <https://doi.org/10.1021/la204855j>.
- [40] T. Abraham, Effects of divalent salt on adsorption kinetics of a hydrophobically modified polyelectrolyte at the neutral surface - aqueous solution interface, Polymer (Guildf). 43 (2002) 849–855.
- [41] S. Mulyati, R. Takagi, A. Fujii, Y. Ohmukai, T. Maruyama, H. Matsuyama, Improvement of the antifouling potential of an anion exchange membrane by surface modification with a polyelectrolyte for an electro dialysis process, J. Memb. Sci. 417–418 (2012) 137–143, <https://doi.org/10.1016/j.memsci.2012.06.024>.
- [42] Y. Zhang, M. Tirrell, J.W. Mays, Effects of ionic strength and counterion valency on adsorption of hydrophobically modified polyelectrolytes, Macromolecules. 29 (1996) 7299–7301, <https://doi.org/10.1021/ma960214u>.
- [43] M. Bjørsvik, H. Høiland, A. Skauge, Formation of colloidal dispersion gels from aqueous polyacrylamide solutions, Colloids Surfaces Physicochem. Eng. Asp. 317 (2008) 504–511, <https://doi.org/10.1016/j.colsurfa.2007.11.025>.
- [44] P.-Y. Ben Jar, Y.S. Wu, Effect of counter-ions on swelling and shrinkage of polyacrylamide-based ionic gels, Polymer (Guildf) 38 (1997) 2557–2560.
- [45] T. Tanaka, I. Nishio, S.-T. Sun, S. Ueno-Nishio, Collapse of gels in an electric field, Science (80-) 218 (4571) (1982) 467–469.
- [46] S. Choi, pH Sensitive polymers for novel conformance control and polymer flooding applications, The University of Texas at Austin, 2008.
- [47] M. Dudek, E. Kancir, G. Øye, Influence of the crude oil and water compositions on the quality of synthetic produced water, Energy and Fuels. 31 (2017) 3708–3716, <https://doi.org/10.1021/acs.energyfuels.6b03297>.
- [48] N. Tanaka, M. Nagase, M. Higa, Preparation of aliphatic-hydrocarbon-based anion-exchange membranes and their anti-organic-fouling properties, J. Memb. Sci. 384 (2011) 27–36, <https://doi.org/10.1016/j.memsci.2011.08.064>.
- [49] N. Tanaka, M. Nagase, M. Higa, Organic fouling behavior of commercially available hydrocarbon-based anion-exchange membranes by various organic-fouling substances, Desalination 296 (2012) 81–86, <https://doi.org/10.1016/j.desal.2012.04.010>.
- [50] M. Higa, N. Tanaka, M. Nagase, K. Yutani, T. Kameyama, K. Takamura, Y. Kakihana, Electro dialytic properties of aromatic and aliphatic type hydrocarbon-based anion-exchange membranes with various anion-exchange groups, Polymer (Guildf). 55 (2014) 3951–3960, <https://doi.org/10.1016/j.polymer.2014.06.072>.